ARTICLE

Electron-Doping-Enhanced Trion Formation in Monolayer Molybdenum Disulfide Functionalized with Cesium Carbonate

Jia Dan Lin,[†,‡,▲] Cheng Han,[†,‡,▲] Fei Wang,[†,§,▲] Rui Wang,[‡] Du Xiang,[‡] Shiqiao Qin,[†] Xue-Ao Zhang,[†,*] Li Wang,[⊥] Hua Zhang,[‖] Andrew Thye Shen Wee,[‡,#] and Wei Chen[‡,¶,#,*]

[†]College of Science, National University of Defense Technology, Changsha 410073, China, [‡]Department of Physics, National University of Singapore, 2 Science Drive 3, Singapore 117542, [§]College of Physics and Electronics, Central South University, Changsha, Hunan 410073, China, [⊥]Institute for Advanced Study and Department of Physics, Nanchang University, 999 Xue Fu Da Dao, Nanchang, China, [‖]School of Materials Science and Engineering, Nanyang Technological University, 50 Nanyang Avenue, Singapore 639798, [¶]Department of Chemistry, National University of Singapore, 3 Science Drive 3, Singapore 117543, and [#]Graphene Research Centre, National University of Singapore, 2 Science Drive 3, Singapore 117542. [▲]These authors contributed equally to this work.

ABSTRACT We report effective and stable electron doping of monolayer molybdenum disulfide (MoS_2) by cesium carbonate (Cs_2CO_3) surface functionalization. The electron charge carrier concentration in exfoliated monolayer MoS_2 can be increased by about 9 times after Cs_2CO_3 functionalization. The n-type doping effect was evaluated by *in situ* transport measurements of MoS_2 field-effect transistors (FETs) and further corroborated by *in situ* ultraviolet photoelectron spectroscopy, X-ray photoelectron spectroscopy, and Raman scattering measurements. The electron doping enhances the formation of negative trions (*i.e.*, a quasiparticle comprising two electrons and one hole) in monolayer MoS_2 under light irradiation and significantly reduces the charge recombination of photoexcited electron−hole pairs. This results in large photoluminescence suppression and an obvious photocurrent enhancement in monolayer MoS_2 FETs.

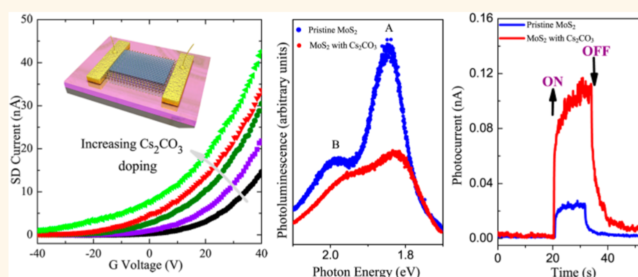

KEYWORDS: MoS_2 · FET · n-type doping · Cs_2CO_3 · photoluminescence · Raman · photocurrent

Layered metal dichalcogenides (LMDCs), in particular, molybdenum disulfide (MoS_2), have attracted much attention for their potential applications as electrocatalysts for hydrogen evolution, logic circuits, optoelectronic devices, and "valleytronics".[1−17] The MoS_2 crystal is formed by layers consisting of two sheets of S atoms and one sheet of Mo atoms that are hexagonally packed.[18] As adjacent layers in MoS_2 crystals are bound together by weak van der Waals forces,[19] mono- or few-layer MoS_2 can be fabricated by micromechanical cleavage, liquid-phase preparation, or intercalation-assisted exfoliation.[20,21] Large-area ultrathin MoS_2 layers synthesized by chemical vapor deposition[22,23] have also been recently demonstrated.

Monolayer MoS_2 has dramatically different electronic and optical properties as compared to bulk MoS_2. Bulk MoS_2 is an indirect gap semiconductor with a band gap of ∼1.2 eV, while monolayer MoS_2 is a direct-gap (∼1.8 eV) semiconductor due to quantum confinement effects.[19,24] Owing to the indirect−direct gap transition, enhanced photoluminescence in monolayer MoS_2 has been observed.[25] It has recently been demonstrated that electrons can tightly bind with photoexcited electron−hole pairs to form negative trions in monolayer MoS_2,[26] a quasiparticle comprising two electrons and one hole. The formation of trions can effectively modulate the photoluminescence in monolayer MoS_2.[26] This suggests that the optical properties in monolayer MoS_2 can be manipulated by controlled electron or hole doping, such as *via* electrostatic doping by applying a gate voltage in field-effect transistor (FET) configuration[26,27] or *via* chemical/physical adsorption of electron-withdrawing/donating surface layers.[28−34]

* Address correspondence to xazhang@nudt.edu.cn (X.-A.Z), phycw@nus.edu.sg (W.C).

Received for review March 21, 2014 and accepted April 29, 2014.

Published online May 01, 2014
10.1021/nn501580c

© 2014 American Chemical Society

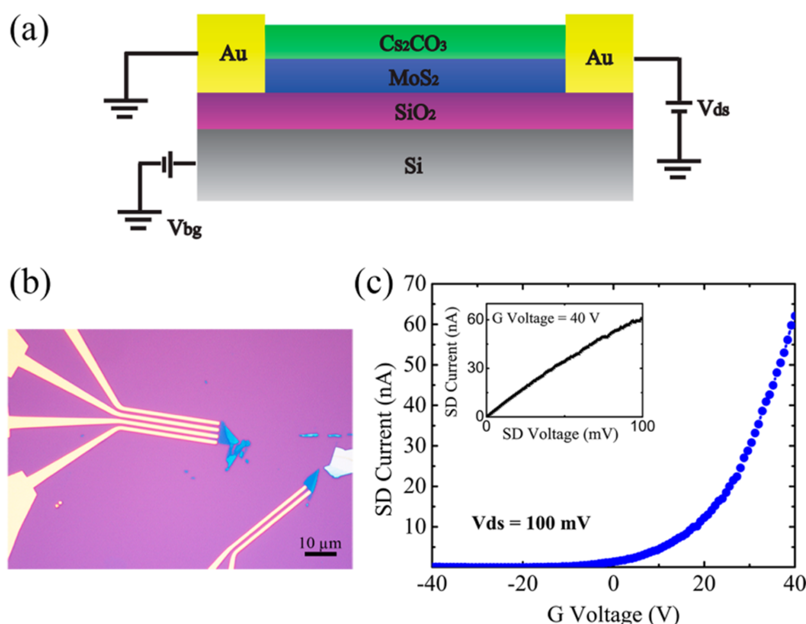

Figure 1. (a) Schematic illustration of the MoS_2 FET layout with Cs_2CO_3 film on top. (b) Optical microscope image of one fabricated device. (c) Transfer characteristic ($I_{ds}-V_g$) of the MoS_2 FET, where V_{ds} = 100 mV. Inset: Output curve ($I_{ds}-V_{ds}$) acquired for V_g value of 40 V.

It was also found that the coupling between electron and phonon can strongly influence the phonon frequencies,[27,29] making the A_{1g} phonon mode extremely sensitive to the electron concentration in monolayer MoS_2. Therefore, controlled doping (electron or hole) can precisely tune both the electronic and optical properties in monolayer MoS_2, hence optimizing the optoelectronic device performance.

One approach to effectively dope MoS_2 predicted by density functional theory is to substitute a S atom with elements from the halogen family (namely, F, Cl, Br, and I) or substitute Mo with transition metals.[34] Although substitutional doping forms a stable system, the structure of MoS_2 is inevitably disturbed by induced defects. Another approach is to physically adsorb gaseous molecules on MoS_2.[28] However, the physically absorbed molecules can be easily desorbed, making it difficult to realize a stable doped MoS_2 system. Chemical doping[31,34−36] is considerably simple, effective, and a high-throughput doping method to tailor the properties of various materials. Recently, Hui *et al.* reported the first degenerate n-doping of few-layer MoS_2-based FET using potassium (K).[33] Cs_2CO_3 is an efficient electron injection material in organic light-emitting devices (OLEDs) and can induce strong n-doping effect in various organic semiconductors.[37−43] In this article, we report the effective and stable electron doping (n-type doping) of monolayer MoS_2 *via* surface functionalization using cesium carbonate (Cs_2CO_3), corroborated by the combination of *in situ* FET device evaluation, *in situ* ultraviolet photoelectron spectroscopy (UPS), and X-ray photoelectron spectroscopy (XPS). The surface

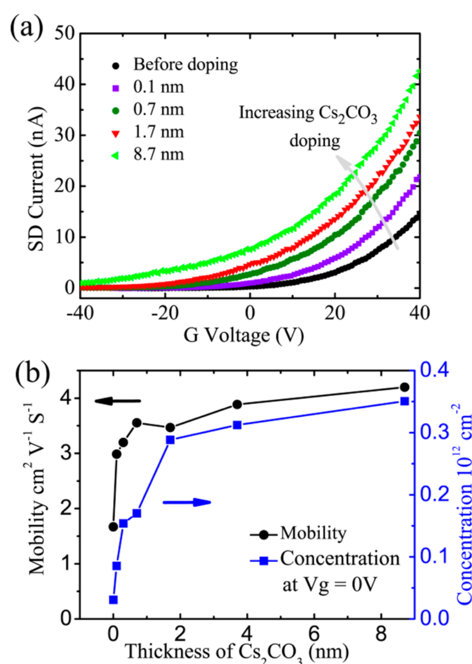

Figure 2. (a) Transfer characteristics of the same MoS_2 FET in high vacuum with increasing thickness of Cs_2CO_3 overlayers (V_{ds} = 100 mV). (b) Estimated field-effect mobility and electron concentration at V_g = 0 V as a function of the Cs_2CO_3 film thickness.

functionalization of Cs_2CO_3 can significantly increase the electron concentration in monolayer MoS_2. These excess electrons can tightly bind with the photoexcited electron−hole pairs to form trions, thereby resulting in a strong suppression of the photoluminescence intensity and a corresponding enhancement of the photocurrent in monolayer MoS_2.

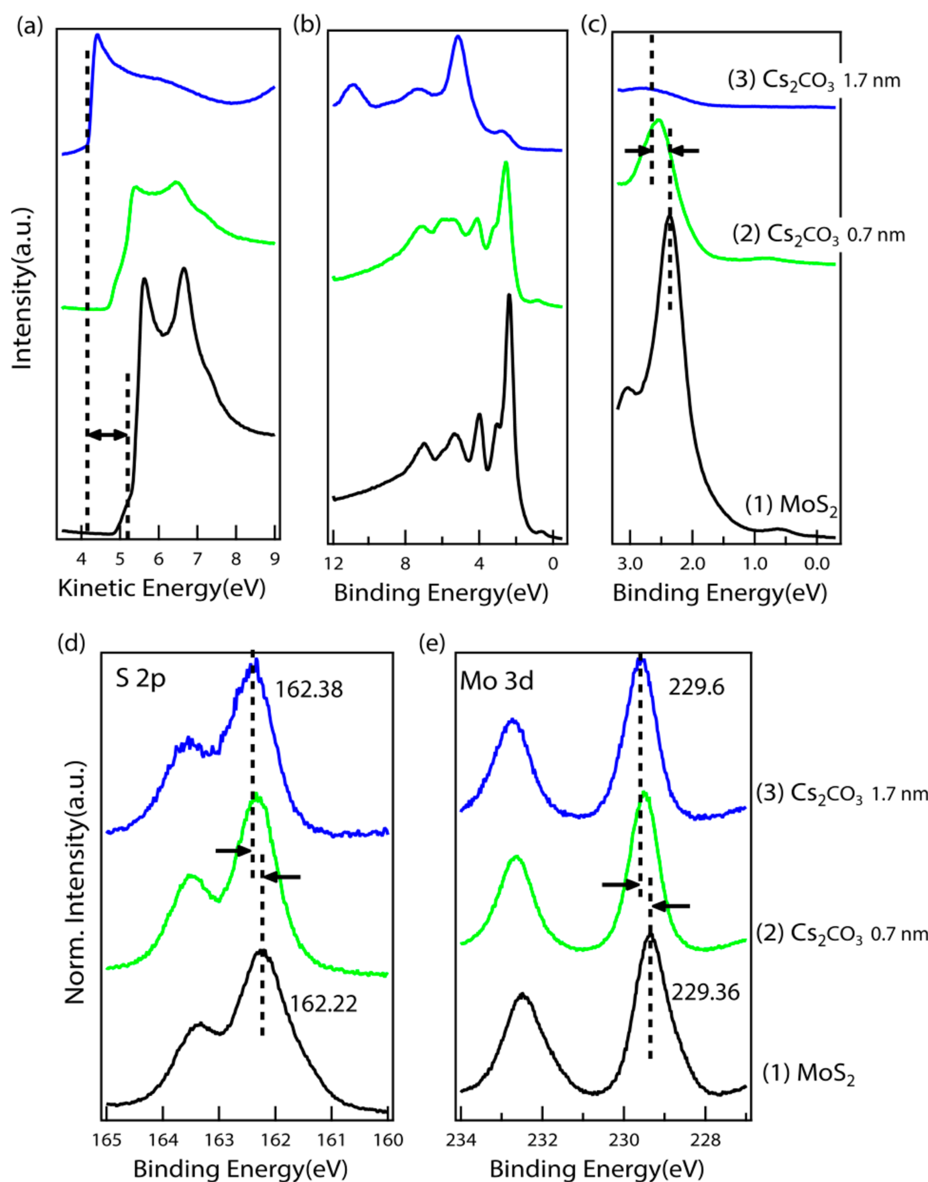

Figure 3. (a−c) UPS spectra at (a) low kinetic energy (secondary electron cutoff) and (b,c) low binding energy region (near the E_F) during the deposition of Cs_2CO_3 on bulk MoS_2. The XPS core level spectra of (d) S 2p and (e) Mo 3d during the deposition of Cs_2CO_3 on bulk MoS_2.

RESULTS AND DISCUSSION

Figure 1a shows a typical bottom-gated MoS_2 FET device with a Cs_2CO_3 surface functionalization layer used in all electrical measurements. The optical microscope image of an as-made MoS_2 FET device is shown in Figure 1b. Figure 1c shows a representative transfer curve (source−drain current as the function of gate voltage: $I_{ds}-V_g$) of the MoS_2 FETs measured in vacuum, exhibiting a typical n-type behavior and consistent with previous reports.[8,31] The output curve (source−drain current as the function of source−drain voltage: $I_{ds}-V_{ds}$) at V_g = 40 V in the inset reveals an ohmic contact behavior.

To examine the effect of Cs_2CO_3 surface functionalization on the electrical transport properties of monolayer MoS_2 FETs, Cs_2CO_3 films with variable thicknesses from 0 to 8.7 nm were evaporated *in situ* on top of the MoS_2 FET. Figure 2a shows the transfer characteristics of a monolayer MoS_2 bottom-gated FET device decorated with Cs_2CO_3 overlayers with different thicknesses measured in high vacuum, revealing obvious n-type doping of MoS_2. From Figure 2a, we estimated the field-effect mobility and electron concentration at V_g = 0 V as a function of the Cs_2CO_3 layer thickness, as shown in Figure 2b. The field-effect electron mobility μ was extracted using the equation $\mu = (L/W)/(\varepsilon_0\varepsilon_r/d) \times (dI_{ds}/dV_g)/V_{ds}$ by fitting the linear regime of the transfer curves in Figure 2a, where L and W are the respective channel length and width, vacuum permittivity, ε_0 = 8.854 × 10^{-12} F m^{-1}, relative permittivity of SiO_2, ε_r = 3.9, and thickness of SiO_2, d = 300 nm. The electron concentration n can be calculated from the field-effect

mobility μ using the relation $\mu = 1/(nq\rho)$, where ρ is the resistivity of the MoS_2 channel. As expected, the electron concentration rose rapidly with increasing Cs_2CO_3 thickness, revealling effective n-type doping of monolayer MoS_2 *via* Cs_2CO_3 surface functionaliztion. Interestingly, the field-effect mobility was also enhanced with inceasing Cs_2CO_3 thickness. Five different MoS_2 samples were used for Cs_2CO_3 doping experiments, and all showed very similar transport behavior. We propose that the field-effect mobility enhancement was caused by the Cs_2CO_3 decoration, which can significantly weaken the scattering effect from the inevitable impurities in pristine MoS_2.

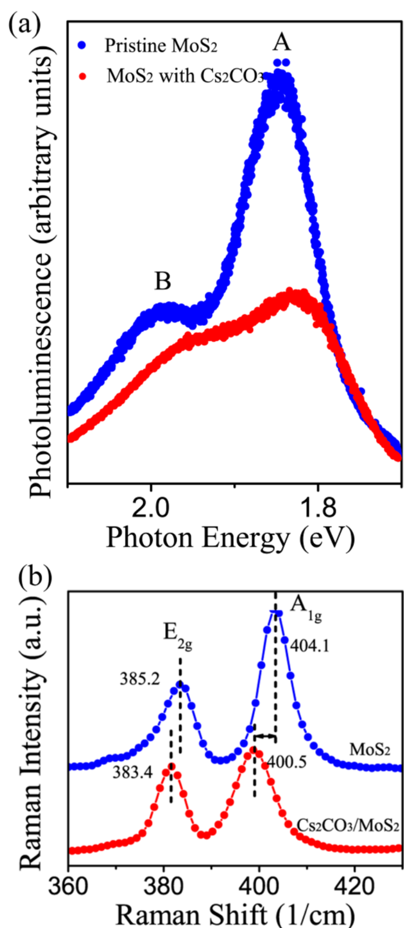

Figure 4. (a) PL and (b) Raman spectra of 1L-MoS_2 before and after Cs_2CO_3 (0.7 nm) doping at room temperature.

To have a better understanding of the n-doping mechanism of MoS_2 using Cs_2CO_3 surface functionalization, *in situ* UPS/XPS measurements were performed to study the interfacial electronic structure at the Cs_2CO_3 and bulk MoS_2 interface. Thickness-dependent UPS spectral evolution of Cs_2CO_3 on bulk MoS_2 is shown in Figure 3a–c and Supporting Information Figure S1. With increasing coverage of Cs_2CO_3 on MoS_2, there was a gradual shift of secondary electron cutoff toward lower kinetic energy (Figure 3a) or a significant reduction of the work function of MoS_2 from 4.50 eV (pristine MoS_2) to 3.46 eV with the decoration of 1.7 nm Cs_2CO_3. The low work function of Cs_2CO_3 facilitates a significant interfacial electron transfer from Cs_2CO_3 overlayers to the underlying MoS_2 once the physical contact is established. As a result, an apparent vacuum level shift or interface dipole was observed at the interface. As shown in Figure 3b,c, this work function reduction was accompanied by a downward band-bending of the MoS_2-related valence band toward higher binding energy. Figure 3d,e presents the S 2p and Mo 3d core level spectra at selected thicknesses of Cs_2CO_3 on bulk MoS_2. The S $2p_{3/2}$ peak shifted from 162.22 to 162.38 eV, and the Mo $3d_{5/2}$ peak shifted from 229.36 to 229.60 eV. The surface charge transfer doping arising from the functionalization of the low work function Cs_2CO_3 can lead to the Fermi level moving toward the conduction band minimum of MoS_2 and band-bending emergence at the interface. Such downward band-bending is consistent with our UPS measurements and further confirms the n-type doping of MoS_2 *via* Cs_2CO_3 surface functionalization.

Figure 4a (blue line) displays a typical photoluminescence spectrum of as-prepared monolayer MoS_2.

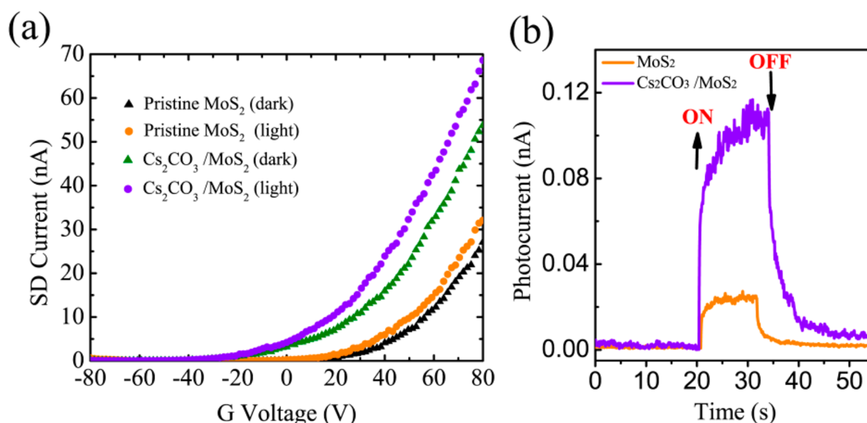

Figure 5. (a) Typical transfer curves ($I_{ds}-V_g$) for the same device under light illumination and dark without and with Cs_2CO_3 decoration. (b) Photocurrent of the device as a function of time of the illumination source at constant optical power without (orange line) and with (violet line) Cs_2CO_3 decoration, respectively (V_{ds} = 20 mV, V_g = 0 V).

Pronounced luminescence emissions were observed at about 1.84 eV (A) and 1.99 eV (B). These two peaks are associated with direct gap transitions from the highest spin−orbital split valence bands at K (K′) point to the lowest conduction bands.[25] After decoration with Cs_2CO_3, the PL peak of monolayer MoS_2 (peak A) was largely suppressed and broadened. The reduction of photoluminescence is attributed primarily to the formation of tightly bound trions.[26,31] The excess electrons induced by Cs_2CO_3 functionalization can effectively bind with photoexcited electron−hole pairs and form the negative trions in monolayer MoS_2, thereby reducing the charge recombination and PL intensity of peak A.[26] This is in good agreement with a recent report of PL spectra change caused by FET back-gate doping.[26]

A typical Raman spectrum of as-prepared monolayer MoS_2 is shown in Figure 4b (blue line). The difference of Raman frequencies between out-of-plane A_{1g} and in-plane E^1_{2g} Raman modes was 18.95 cm^{-1}, confirming the monolayer nature of the MoS_2 sample.[44] The out-of-plane A_{1g} and in-plane E^1_{2g} Raman frequencies were red-shifted after decoration of Cs_2CO_3. The A_{1g} phonon frequency downshifted by 3.6 cm^{-1}, accompanied by a reduction in peak intensity and peak broadening. In contrast, only a 1.7 cm^{-1} frequency shift was observed for the E^1_{2g} phonon with almost unchanged peak intensity and peak full width at half-maximum (fwhm). In monolayer MoS_2, A_{1g} phonons couple much more tightly with electrons than E^1_{2g} phonons.[27,29] Hence, electron doping leads to a significant change in A_{1g} phonon peak, while the E^1_{2g} phonon peak is less affected.

We also evaluated the n-type doping effect on MoS_2-based optoelectronic devices. Photocurrent measurements were carried out using a 514 nm light source with constant optical output power of 5 mW/cm^2 under ambient air conditions. The photocurrent of the MoS_2 device was enhanced about 5 times after decoration with Cs_2CO_3, as shown in Figure 5b. Here, we define the photocurrent as the source−drain current difference with and without light irradiation. We propose that the electron-doping-induced formation of trions can significantly reduce the recombination of photoexcited electron−hole pairs, resulting in photocurrent enhancement in monolayer MoS_2 FET. Moreover, Cs_2CO_3 decoration can effectively reduce impurity scattering in MoS_2 devices, hence improving the electron mobility, thereby enhancing the photocurrent response.

For practical applications, it is crucial to check the air stability of this doping method. Figure 6 shows the air exposure effect on a MoS_2 FET decorated with 7 nm

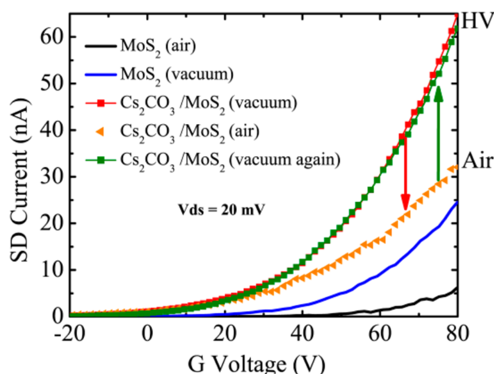

Figure 6. Transfer characteristics of both bottom-gated MoS_2 FETs with 7 nm Cs_2CO_3 and the pristine MoS_2 FET before and after air exposure.

Cs_2CO_3. For comparison, the transfer characteristics of the pristine MoS_2 FET are also presented. For both the MoS_2 device decorated with 7 nm Cs_2CO_3 and the pristine device, the I_{ds} current of both devices dropped after air exposure. However, the n-type doping effect was still very significant compared to pristine MoS_2 FETs in air. Moreover, when we subsequently measured the n-type-doped MoS_2 FET under high vacuum, the I_{ds} current was restored to its original value before air exposure. This indicates that the current drop during the air exposure is mainly attributed to the MoS_2 monolayer. In addition, after the sample was stored in air for 3 days (Figure S3), the doping effect was still considerable, revealing good air stability of n-type doping of MoS_2 by Cs_2CO_3.

CONCLUSION

In conclusion, we demonstrate effective n-type doping of MoS_2 *via* surface functionalization with thermally evaporated Cs_2CO_3 thin films, as revealed by *in situ* transport measurement on MoS_2 FET devices and *in situ* XPS/UPS investigations. After decoration of 1.7 nm Cs_2CO_3, the charge carrier (electron) concentration in MoS_2 increases by about 9 times. The dopant electrons strongly interact with photoexcited electron−hole pairs, leading to the emergence of trions and reduction of photoluminescence. The performance of the MoS_2-based phototransistor is also significantly improved after Cs_2CO_3 decoration. Moreover, the n-type-doped MoS_2 FET device possesses good air stability, which is crucial for practical device applications. This study promises a simple approach to realizing stable n-type doping of 2D materials and tailoring their electronic and optical behavior for future 2D-material-based optoelectronic devices.

MATERIALS AND METHODS

Sample Preparation. Single- and few-layer MoS_2 flakes were mechanically exfoliated from a bulk MoS_2 crystal (SPI Supplies) using adhesive tape and transferred onto Si substrates with a 300 nm thermal oxide adlayer. A high-resolution optical microscope (Nikon Eclipse LV100D) was used to locate and identify

the isolated MoS_2 flakes based on their high optical contrast on 300 nm SiO_2 substrates.

Device Fabrication and Characterization. After mechanical exfoliation of MoS_2 flakes onto Si substrates, PMMA(A7 950) resist was spin-coated on top of the samples. The source and drain electrodes were patterned by conventional electron-beam lithography (FEI Nova NanoSEM 230) followed by a developing process. Cr/Au (5/50 nm) was deposited by thermal evaporation (Nano36) followed by liftoff in hot acetone, cleaning by IPA and drying under N_2. The as-made MoS_2 FETs were wire-bonded and loaded into a high-vacuum chamber (base pressure 10^{-7} mbar) custom designed for room temperature electrical measurements. The electrical transport measurements were performed using an Agilent 2912A precision source/measurement unit. The Cs_2CO_3 was thermally evaporated *in situ* from a Knudsen cell onto the loaded MoS_2 devices in the high-vacuum chamber. The thickness of Cs_2CO_3 layer on the as-made devices was monitored by a quartz crystal microbalance (QCM). Photocurrent measurements on the MoS_2 transistor were performed using a 514 nm light source under constant optical power (5 mW/cm^2).

Photoluminescence and Raman Spectroscopy. Photoluminescence and Raman measurements were performed using a single-mode solid-state laser (532 nm) under ambient conditions (Alpha 300 R). The Raman peak of Si at 520 cm^{-1} was used as a reference for calibration.

XPS and UPS Measurements. *In situ* UPS/XPS experiments of Cs_2CO_3 on bulk MoS_2 were carried out in our custom-built ultra-high-vacuum system with He I (21.2 eV) and Mg Kα (1253.6 eV) as excitation sources, respectively. The nominal thickness of Cs_2CO_3 was estimated by monitoring the attenuation of the S 2p peak intensity of bulk MoS_2 crystal before and after deposition and further calibrated by QCM. The binding energy of all XPS/UPS spectra was calibrated to the Fermi level of a sputter-cleaned Ag substrate. A -5 V sample bias was applied during secondary electron cutoff measurements of UPS spectra to reveal the change of the sample work function.

Conflict of Interest: The authors declare no competing financial interest.

Acknowledgment. Authors acknowledge the technical support from NUS Graphene Research Centre for the device fabrication, and financial support from Singapore MOE Grants R143-000-505-112, R143-000-530-112, R143-000-542-112, and R143-000-559-112.

Supporting Information Available: Figure S1: Thickness-dependent UPS/XPS spectra during the deposition of Cs_2CO_3 on bulk MoS_2. The thickness of Cs_2CO_3 was gradually increased from 0 to 1.7 nm. Figure S2: Optical microscope image and Raman spectrum of the single-layer MoS_2 on a 300 nm SiO_2/Si substrate. Figure S3: Transfer characteristics of bottom-gated MoS_2 FETs with 7 nm Cs_2CO_3 exposed in air for 3 days compared to the pristine MoS_2 FETs tested in vacuum. This material is available free of charge *via* the Internet at http://pubs.acs.org.

REFERENCES AND NOTES

1. Butler, S. Z.; Hollen, S. M.; Cao, L.; Cui, Y.; Gupta, J. A.; Gutiérrez, H. R.; Heinz, T. F.; Hong, S. S.; Huang, J.; Ismach, A. F.; *et al.* Progress, Challenges, and Opportunities in Two-Dimensional Materials Beyond Graphene. *ACS Nano* **2013**, *7*, 2898–2926.
2. Chhowalla, M.; Shin, H. S.; Eda, G.; Li, L.-J.; Loh, K. P.; Zhang, H. The Chemistry of Two-Dimensional Layered Transition Metal Dichalcogenide Nanosheets. *Nat. Chem.* **2013**, *5*, 263–275.
3. Fang, H.; Chuang, S.; Chang, T. C.; Takei, K.; Takahashi, T.; Javey, A. High-Performance Single Layered WSe_2 p-FETs with Chemically Doped Contacts. *Nano Lett.* **2012**, *12*, 3788–3792.
4. Gutiérrez, H. R.; Perea-López, N.; Elías, A. L.; Berkdemir, A.; Wang, B.; Lv, R.; López-Urías, F.; Crespi, V. H.; Terrones, H.; Terrones, M. Extraordinary Room-Temperature Photoluminescence in Triangular WS_2 Monolayers. *Nano Lett.* **2013**, *13*, 3447–3454.
5. Wang, Q. H.; Kalantar-Zadeh, K.; Kis, A.; Coleman, J. N.; Strano, M. S. Electronics and Optoelectronics of Two-Dimensional Transition Metal Dichalcogenides. *Nat. Nanotechnol.* **2012**, *7*, 699–712.
6. Xiao, D.; Liu, G.-B.; Feng, W.; Xu, X.; Yao, W. Coupled Spin and Valley Physics in Monolayers of MoS_2 and Other Group-VI Dichalcogenides. *Phys. Rev. Lett.* **2012**, *108*, 196802.
7. Yin, Z. Y.; Li, H.; Li, H.; Jiang, L.; Shi, Y. M.; Sun, Y. H.; Lu, G.; Zhang, Q.; Chen, X. D.; Zhang, H. Single-Layer MoS_2 Phototransistors. *ACS Nano* **2012**, *6*, 74–80.
8. Lin, J.; Li, H.; Zhang, H.; Chen, W. Plasmonic Enhancement of Photocurrent in MoS_2 Field-Effect-Transistor. *Appl. Phys. Lett.* **2013**, *102*, 203109.
9. Lee, H. S.; Min, S.-W.; Chang, Y.-G.; Park, M. K.; Nam, T.; Kim, H.; Kim, J. H.; Ryu, S.; Im, S. MoS_2 Nanosheet Phototransistors with Thickness-Modulated Optical Energy Gap. *Nano Lett.* **2012**, *12*, 3695–3700.
10. Kibsgaard, J.; Chen, Z. B.; Reinecke, B. N.; Jaramillo, T. F. Engineering the Surface Structure of MoS_2 To Preferentially Expose Active Edge Sites for Electrocatalysis. *Nat. Mater.* **2012**, *11*, 963–969.
11. Zong, X.; Wu, G. P.; Yan, H. J.; Ma, G. J.; Shi, J. Y.; Wen, F. Y.; Wang, L.; Li, C. Photocatalytic H_2 Evolution on MoS_2/CdS Catalysts under Visible Light Irradiation. *J. Phys. Chem. C* **2010**, *114*, 1963–1968.
12. Radisavljevic, B.; Radenovic, A.; Brivio, J.; Giacometti, V.; Kis, A. Single-Layer MoS_2 Transistors. *Nat. Nanotechnol.* **2011**, *6*, 147–150.
13. Yu, W. J.; Li, Z.; Zhou, H.; Chen, Y.; Wang, Y.; Huang, Y.; Duan, X. Vertically Stacked Multi-heterostructures of Layered Materials for Logic Transistors and Complementary Inverters. *Nat. Mater.* **2013**, *12*, 246–252.
14. Mak, K. F.; He, K.; Shan, J.; Heinz, T. F. Control of Valley Polarization in Monolayer MoS_2 by Optical Helicity. *Nat. Nanotechnol.* **2012**, *7*, 494–498.
15. Huang, X.; Zeng, Z. Y.; Zhang, H. Metal Dichalcogenide Nanosheets: Preparation, Properties and Applications. *Chem. Soc. Rev.* **2013**, *42*, 1934–1946.
16. Huang, X.; Tan, C. L.; Yin, Z. Y.; Zhang, H. 25th Anniversary Article: Hybrid Nanostructures Based on Two-Dimensional Nanomaterials. *Adv. Mater.* **2014**, *26*, 2185–2204.
17. Huang, X.; Zeng, Z. Y.; Bao, S. Y.; Wang, M. F.; Qi, X. Y.; Fan, Z. X.; Zhang, H. Solution-Phase Epitaxial Growth of Noble Metal Nanostructures on Dispersible Single-Layer MoS_2 Nanosheets. *Nat. Commun.* **2013**, *4*, 1444.
18. Kasowski, R. Band Structure of MoS_2 and NbS_2. *Phys. Rev. Lett.* **1973**, *30*, 1175–1178.
19. Lebègue, S.; Eriksson, O. Electronic Structure of Two-Dimensional Crystals from *Ab Initio* Theory. *Phys. Rev. B* **2009**, *79*, 115409.
20. Lee, K.; Kim, H.-Y.; Lotya, M.; Coleman, J. N.; Kim, G.-T.; Duesberg, G. S. Electrical Characteristics of Molybdenum Disulfide Flakes Produced by Liquid Exfoliation. *Adv. Mater.* **2011**, *23*, 4178–4182.
21. Zeng, Z.; Yin, Z.; Huang, X.; Li, H.; He, Q.; Lu, G.; Boey, F.; Zhang, H. Single-Layer Semiconducting Nanosheets: High-Yield Preparation and Device Fabrication. *Angew. Chem., Int. Ed.* **2011**, *50*, 11093–11097.
22. Lee, Y.-H.; Zhang, X.-Q.; Zhang, W.; Chang, M.-T.; Lin, C.-T.; Chang, K.-D.; Yu, Y.-C.; Wang, J. T.-W.; Chang, C.-S.; Li, L.-J.; *et al.* Synthesis of Large-Area MoS_2 Atomic Layers with Chemical Vapor Deposition. *Adv. Mater.* **2012**, *24*, 2320–2325.
23. Shi, Y.; Zhou, W.; Lu, A.-Y.; Fang, W.; Lee, Y.-H.; Hsu, A. L.; Kim, S. M.; Kim, K. K.; Yang, H. Y.; Li, L.-J.; *et al.* van der Waals Epitaxy of MoS_2 Layers Using Graphene as Growth Templates. *Nano Lett.* **2012**, *12*, 2784–2791.
24. Mak, K. F.; Lee, C.; Hone, J.; Shan, J.; Heinz, T. F. Atomically Thin MoS_2: A New Direct-Gap Semiconductor. *Phys. Rev. Lett.* **2010**, *105*, 136805.
25. Splendiani, A.; Sun, L.; Zhang, Y.; Li, T.; Kim, J.; Chim, C.-Y.; Galli, G.; Wang, F. Emerging Photoluminescence in Monolayer MoS_2. *Nano Lett.* **2010**, *10*, 1271–1275.

26. Mak, K. F.; He, K.; Lee, C.; Lee, G. H.; Hone, J.; Heinz, T. F.; Shan, J. Tightly Bound Trions in Monolayer MoS_2. *Nat. Mater.* **2013**, *12*, 207–211.
27. Chakraborty, B.; Bera, A.; Muthu, D. V. S.; Bhowmick, S.; Waghmare, U. V.; Sood, A. K. Symmetry-Dependent Phonon Renormalization in Monolayer MoS_2 Transistor. *Phys. Rev. B* **2012**, *85*, 161403.
28. Tongay, S.; Zhou, J.; Ataca, C.; Liu, J.; Kang, J. S.; Matthews, T. S.; You, L.; Li, J.; Grossman, J. C.; Wu, J. Broad-Range Modulation of Light Emission in Two-Dimensional Semiconductors by Molecular Physisorption Gating. *Nano Lett.* **2013**, *13*, 2831–2836.
29. Dey, S.; Matte, H. S. S. R.; Shirodkar, S. N.; Waghmare, U. V.; Rao, C. N. R. Charge-Transfer Interaction between Few-Layer MoS_2 and Tetrathiafulvalene. *Chem.—Asian J.* **2013**, *8*, 1780–1784.
30. Ross, J. S.; Wu, S.; Yu, H.; Ghimire, N. J.; Jones, A. M.; Aivazian, G.; Yan, J.; Mandrus, D. G.; Xiao, D.; Yao, W.; *et al.* Electrical Control of Neutral and Charged Excitons in a Monolayer Semiconductor. *Nat. Commun.* **2013**, *4*, 1474.
31. Mouri, S.; Miyauchi, Y.; Matsuda, K. Tunable Photoluminescence of Monolayer MoS_2 *via* Chemical Doping. *Nano Lett.* **2013**, *13*, 5944–5948.
32. Lin, J.; Zhong, J.; Zhong, S.; Li, H.; Zhang, H.; Chen, W. Modulating Electronic Transport Properties of MoS_2 Field Effect Transistor by Surface Overlayers. *Appl. Phys. Lett.* **2013**, *103*, 063109.
33. Fang, H.; Tosun, M.; Seol, G.; Chang, T. C.; Takei, K.; Guo, J.; Javey, A. Degenerate n-Doping of Few-Layer Transition Metal Dichalcogenides by Potassium. *Nano Lett.* **2013**, *13*, 1991–1995.
34. Dolui, K.; Rungger, I.; Pemmaraju, C. D.; Sanvito, S. Possible Doping Strategies for MoS_2 Monolayers: An *Ab Initio* Study. *Phys. Rev. B* **2013**, *88*, 075420.
35. Perkins, F. K.; Friedman, A. L.; Cobas, E.; Campbell, P. M.; Jernigan, G. G.; Jonker, B. T. Chemical Vapor Sensing with Monolayer MoS_2. *Nano Lett.* **2013**, *13*, 668–673.
36. Du, Y.; Liu, H.; Neal, A. T.; Si, M.; Ye, P. D. Molecular Doping of Multilayer MoS_2 Field-Effect Transistors Reduction in Sheet and Contact Resistance. *IEEE Electron Device Lett.* **2013**, *34*, 1328–1330.
37. Wu, C.-I.; Lin, C.-T.; Chen, Y.-H.; Chen, M.-H.; Lu, Y.-J.; Wu, C.-C. Electronic Structures and Electron-Injection Mechanisms of Cesium-Carbonate-Incorporated Cathode Structures for Organic Light-Emitting Devices. *Appl. Phys. Lett.* **2006**, *88*, 152104.
38. Li, G.; Chu, C. W.; Shrotriya, V.; Huang, J.; Yang, Y. Efficient Inverted Polymer Solar Cells. *Appl. Phys. Lett.* **2006**, *88*, 253503.
39. Huang, J.; Watanabe, T.; Ueno, K.; Yang, Y. Highly Efficient Red-Emission Polymer Phosphorescent Light-Emitting Diodes Based on Two Novel Tris(1-phenylisoquinolinato-C2,N)iridium(III) Derivatives. *Adv. Mater.* **2007**, *19*, 739–743.
40. Liao, H.-H.; Chen, L.-M.; Xu, Z.; Li, G.; Yang, Y. Highly Efficient Inverted Polymer Solar Cell by Low Temperature Annealing of Cs_2CO_3 Interlayer. *Appl. Phys. Lett.* **2008**, *92*, 173303.
41. Huang, J.; Li, G.; Yang, Y. A Semi-transparent Plastic Solar Cell Fabricated by a Lamination Process. *Adv. Mater.* **2008**, *20*, 415–419.
42. Huang, J.; Xu, Z.; Yang, Y. Low-Work-Function Surface Formed by Solution-Processed and Thermally Deposited Nanoscale Layers of Cesium Carbonate. *Adv. Funct. Mater.* **2007**, *17*, 1966–1973.
43. Xu, Z.; Chen, L.-M.; Yang, G.; Huang, C.-H.; Hou, J.; Wu, Y.; Li, G.; Hsu, C.-S.; Yang, Y. Vertical Phase Separation in Poly(3-hexylthiophene): Fullerene Derivative Blends and Its Advantage for Inverted Structure Solar Cells. *Adv. Funct. Mater.* **2009**, *19*, 1227–1234.
44. Lee, C.; Yan, H.; Brus, L. E.; Heinz, T. F.; Hone, J.; Ryu, S. Anomalous Lattice Vibrations of Single- and Few-Layer MoS_2. *ACS Nano* **2010**, *4*, 2695–2700.